JOURNAL OF GUIDANCE, CONTROL, AND DYNAMICS
Vol. 30, No. 3, May–June 2007

Control-Oriented Modeling of an Air-Breathing Hypersonic Vehicle

Jason T. Parker*
U.S. Air Force Research Laboratory, Wright–Patterson Air Force Base, Ohio 45433
Andrea Serrani† and Stephen Yurkovich‡
The Ohio State University, Columbus, Ohio 43210
and
Michael A. Bolender§ and David B. Doman¶
U.S. Air Force Research Laboratory, Wright–Patterson Air Force Base, Ohio, 45433

DOI: 10.2514/1.27830

Full simulation models for flexible air-breathing hypersonic vehicles include intricate couplings between the engine and flight dynamics, along with complex interplay between flexible and rigid modes, resulting in intractable systems for nonlinear control design. In this paper, starting from a high-fidelity model, a control-oriented model in closed form is obtained by replacing complex force and moment functions with curve-fitted approximations, neglecting certain weak couplings, and neglecting slower portions of the system dynamics. The process itself allows an understanding of the system-theoretic properties of the model, and enables the applicability of model-based nonlinear control techniques. Although the focus of this paper is on the development of the control-oriented model, an example of control design based on approximate feedback linearization is provided. Simulation results demonstrate that this technique achieves excellent tracking performance, even in the presence of moderate parameter variations. The fidelity of the truth model is then increased by including additional flexible effects, which render the original control design ineffective. A more elaborate model with an additional actuator is then employed to enhance the control authority of the vehicle, required to compensate for the new flexible effects, and a new design is provided.

Nomenclature

$A(\cdot)$	=	decoupling matrix of Lie derivatives
$C_D(\alpha, \delta_e)$	=	drag coefficient
$C_D^{\alpha^i}$	=	ith order coefficient of α contribution to $C_D(\alpha, \delta_e)$
$C_D^{\delta_e^i}$	=	ith order coefficient of δ_e contribution to $C_D(\alpha, \delta_e)$
C_D^0	=	constant term in $C_D(\alpha, \delta_e)$
$C_L(\alpha, \delta_e)$	=	lift coefficient
$C_L^{\alpha^i}$	=	ith order coefficient of α contribution to $C_L(\alpha, \delta_e)$
$C_L^{\delta_e}$	=	coefficient of δ_e contribution to $C_L(\alpha, \delta_e)$
C_L^0	=	constant term in $C_L(\alpha, \delta_e)$
$C_{M,Q}(\alpha, Q)$	=	contribution to moment due to pitch rate
$C_{M,\alpha}(\alpha)$	=	contribution to moment due to angle of attack
$C_{M,\delta_e}(\delta_e, \delta_c)$	=	control surfaces contribution to moment
$C_{M,\alpha}^{\alpha^i}$	=	ith order coefficient of α contribution to $C_{M,\alpha}(\alpha)$
$C_{M,\alpha}^0$	=	constant term in $C_{M,\alpha}(\alpha)$
$C_T^{\alpha^i}(\Phi)$	=	ith order coefficient of α in T
$\bar{c}$	=	mean aerodynamic chord
c_c	=	canard coefficient in $C_{M,\delta_e}(\delta_e, \delta_c)$
c_e	=	elevator coefficient in $C_{M,\delta_e}(\delta_e, \delta_c)$
D	=	drag
F_x	=	x_B direction force component
F_z	=	z_B direction force component
g	=	acceleration due to gravity
h	=	altitude
h_{ref}	=	altitude reference trajectory
h_0	=	nominal altitude for air density approximation
I_{yy}	=	moment of inertia
K_V	=	LQR gain for outer-loop V controller
K_γ	=	LQR gain for outer-loop γ controller
k_{ec}	=	Eelevator/canard interconnection gain
k_i	=	$1 + \tilde{\psi}_i / I_{yy}$
L	=	lift
L_v	=	vehicle length
$\mathcal{L}_f\varphi$	=	Lie derivative of the function φ along the vector field f
M	=	pitching moment
M_∞	=	freestream Mach number
m	=	vehicle mass
N_i	=	ith generalized force
$N_i^{\alpha^j}$	=	jth order contribution of α to N_i
N_i^0	=	constant term in N_i
$N_2^{\delta_e}$	=	contribution of δ_e to N_2
Q	=	pitch rate
Q_V	=	LQR design weight for V loop
Q_γ	=	LQR design weight for γ loop
$\bar{q}$	=	dynamic pressure
R_V	=	LQR control weight for V loop
R_γ	=	LQR control weight for γ loop
S	=	reference area
T	=	thrust
U	=	velocity component in the x_B direction
u_V	=	control input for outer V loop

Presented as Paper 6556 at the AIAA Guidance, Navigation, and Control Conference and Exhibit, Keystone, CO, 21–24 August 2006; received 14 September 2006; revision received 19 December 2006; accepted for publication 21 December 2006. This material is declared a work of the U.S. Government and is not subject to copyright protection in the United States. Copies of this paper may be made for personal or internal use, on condition that the copier pay the $10.00 per-copy fee to the Copyright Clearance Center, Inc., 222 Rosewood Drive, Danvers, MA 01923; include the code 0731-5090/07 $10.00 in correspondence with the CCC.

*Associate Electronics Engineer, U.S. Air Force Research Laboratory/Radar Signal Processing Technology Branch, 2241 Avionics Circle.
†Assistant Professor, Department of Electrical and Computer Engineering, 2015 Neil Avenue. Member AIAA.
‡Professor, Department of Electrical and Computer Engineering, 2015 Neil Avenue.
§Aerospace Engineer, U.S. Air Force Research Laboratory/Control Design and Analysis Branch, 2210 Eighth Street, Suite 21. Senior Member AIAA.
¶Senior Aerospace Engineer, U.S. Air Force Research Laboratory/Control Design and Analysis Branch, 2210 Eighth Street, Suite 21. Associate Fellow AIAA.

u_γ = control input for outer γ loop
V = velocity
V_{ref} = velocity reference trajectory
W = velocity component in the z_B direction
x = state of the control-oriented model
x_B = body axis coordinate frame x direction
x_{CFM} = state of the curve-fitted model
x_{TM} = state of the truth model
x_{TMH} = state of the truth model with heave coupling
x_0 = trim condition
z = state of the control-oriented model in normal form
z_B = body axis coordinate frame z direction
z_T = thrust to moment coupling coefficient
z_0 = trim condition
α = angle of attack
$\beta_i(h, \bar{q})$ = ith thrust fit parameter
$\Gamma(x)$ = diffeomorphism corresponding to normal form of COM
γ = flight path angle, $\gamma = \theta - \alpha$
γ_{ref} = reference trajectory for γ
ΔT_0 = total temperature change across combustor
δ_c = canard angular deflection
δ_e = elevator angular deflection
ζ = damping ratio for the Φ dynamics
ζ_i = damping ratio for elastic mode η_i
η_i = ith generalized elastic coordinate
θ = pitch angle
λ_i = inertial coupling terms for ith elastic mode
ρ = air density
Φ = stoichiometrically normalized fuel-to-air ratio
Φ_c = commanded value of Φ
$\tilde{\psi}_i$ = constrained beam coupling constant for η_i
ω = natural frequency for the Φ dynamics
ω_i = natural frequency for elastic mode η_i
$1/h_s$ = air density decay rate

Introduction

AIR-BREATHING hypersonic vehicles may eventually allow dramatic reductions in flight times for both commercial and military applications. Direct access to Earth orbit without the use of separate boosting stages may also become possible as scramjet-powered aircraft enter service. Although numerous challenges remain, recent successes with NASA's X-43a and renewed research activities throughout the aerospace community suggest that this technology may be on its way to assuming a role in the next generation of aviation.

The design of guidance and control systems for air-breathing hypersonic vehicles requires the control engineer to deal with strong couplings between propulsive and aerodynamic effects while also addressing the significant flexibility associated with the slender geometries required for these aircraft [1–3]. Most control schemes proposed to date have been limited in their scope to the longitudinal dynamics of hypersonic vehicles. A wide range of control laws have been developed for linearized versions of hypersonic models [1,2,4–6], whereas a few have also attempted to incorporate guidance [7,8]. Tournes et al. employed a nonlinear variable structure control approach in [9], whereas several other nonlinear control approaches have been proposed for nearly nonflexible models [10–13] This paper builds on results presented in [14] and now includes more extensive analysis along with a control design for a more sophisticated version of the model.

Real-world models rarely match the assumptions required for a given control technique. As a result, modifications and/or simplifications must be made to the mathematical model of the plant to allow the application of a given technique, or a new methodology must be devised. This paper chooses the former course to develop a simplified control-oriented version of a rich hypersonic vehicle model. The goal is to demonstrate the effectiveness of modeling specifically for control design and to emphasize the advantages in exploiting the inherent connections between modeling and control. To this end, the presented material tracks the development of two versions of the model, and highlights the required changes to the control-oriented model as the complexity of the original plant is increased. By carefully selecting the simplified version of the model used for design, and by representing the neglected portion of the dynamics as uncertainties or perturbations, the application of well-established nonlinear control techniques, which was previously prevented by the complexity of the original model, becomes a possibility. As an example, a control design based on approximate feedback linearization, a technique that has previously been applied to other aircraft models with good results [15,16], is presented in this paper.

Throughout this document, a variety of models will be considered. Indeed, one focus of this research is the development of simplified models suitable first for analysis and later for control of an original model that is analytically intractable. The term "truth model" will be used to refer to a full simulation model that acts as the plant for verification of the presented control designs. As already mentioned, two truth models will be considered in this document, beginning with the flexible air-breathing hypersonic vehicle developed by Bolender and Doman [3]. In this work, compressible flow theory was employed to obtain a more complex and accurate model than those developed in earlier, similar efforts [18,19]. This first model will be referred to as simply the truth model (TM) and will be used solely for simulation and control design verification. Following the successful design of linear controllers [17] for the TM, the next logical step is the synthesis of a nonlinear control law. The application of nonlinear techniques avoids the need for gain scheduling or other similar techniques by using a globally valid model for control design. In addition, the modeling efforts required to complete a nonlinear design offer insights into the structure of a plant that are lost by taking a simple Jacobian linearization. The more intricate control law also offers the potential for an increased domain of attraction for a stabilized equilibrium and increased robustness. Naturally these benefits are not guaranteed by the mere selection of a nonlinear approach, but the potential for improved performance warrants the exploration of these alternative techniques. In this initial study, a feedback linearization approach will be pursued, because this technique is the simplest one that takes full advantage from the availability of a nonlinear control-oriented model.

Intricate interactions between the structural, aerodynamic, and propulsion system equations in the TM result in exceedingly complex expressions for the aerodynamic forces and coupling terms between the flexible states and the other equations of motion. When written in a form suitable for control, these equations are clearly analytically intractable, even with the aid of a computer algebra system. The first step in the control design process is the creation of a curve-fitted model (CFM), which approximates the behavior of the truth model with reduced complexity. Rather than linearizing the model numerically or attempting to fit a nonlinear model to simulation results, curve fits are calculated directly from the forces and moments included in the truth model. The curve fits can then be used analytically to study the behavior of the model from a control engineer's perspective. The resulting nonlinear CFM is at first glance similar to those given in previous works [11,13]. However, as opposed to the models considered in [11,13], the addition of flexible states, increased complexity of the engine model, and additional parasitic couplings between the control effectors and the aerodynamic forces create an unstable zero dynamics with respect to the controlled variables and drastically increase the complexity of the vehicle's governing equations. The nonminimum phase character of this model stems from the pitch dynamics, which introduce a single positive real transmission zero with the given choice of control input. The resulting system possesses vector relative degree two with 7-D internal dynamics.

Rather than attempting to design a controller directly for this unstable, nonminimum phase system, the model is further simplified to allow the application of approximate feedback linearization techniques [15]. The flexible states, altitude dynamics, and a set of weak couplings are removed from the CFM and treated as a dynamic

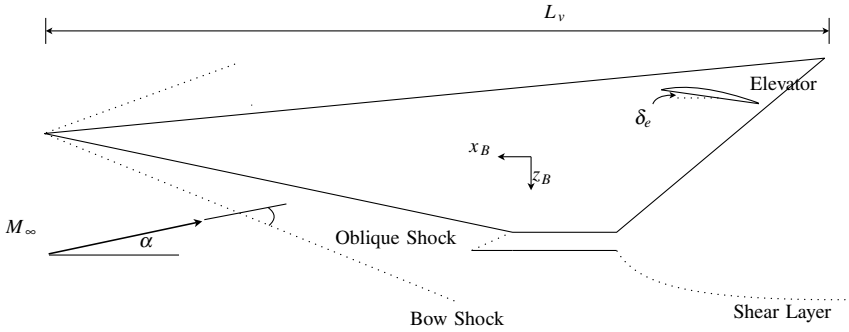

Fig. 1 Geometry of the hypersonic vehicle model.

perturbation to a control-oriented model (COM), which can be shown to possess full vector relative degree with appropriate dynamic extension. Thus, a straightforward design of a feedback linearization control law can be completed for the COM. An outer-loop controller is then designed using linear quadratic regulator (LQR) methods with integral augmentation and a reference model. Simulation studies reveal that, despite the simplification of the plant dynamics, this control law performs well on both the CFM and the TM.

Next, a second, more elaborate, version of the truth model is considered. This model, which includes heave coupling, will be denoted the truth model with heave coupling (TMH). The term heave coupling refers to excitation of the flexible modes by changes in the body axis vertical acceleration. For small values of α, this acceleration is nearly equivalent to $\ddot{h}$. This coupling results in a significantly more complex interconnection between the flexible and rigid dynamics [3]. Unlike the TM, where the only nonminimum phase zero originated from the pitch dynamics, the TMH includes an additional complex conjugate pair of nonminimum phase zeros, which arise due to the increased excitation of the flexible states. As a result, the COM no longer constitutes a valid approximation of the model, and the control law designed on the basis of the COM is unable to stabilize the TMH. It has been recognized that to overcome these difficulties, which manifest themselves in linearized models as well, the control authority should be enhanced by an additional control effector, specifically a canard [20]. In the cited reference, the canard is used to suppress the nonminimum phase behavior of a linearized version of the TMH. Here, this modification is incorporated in a new version of the COM, and used to partially cancel the coupling of the elevator deflection to the lift force, while its contribution to the other aerodynamic forces is accounted for by a modified curve-fitted model. It is shown that, by ganging the canard with the elevator and carefully tuning the relative gain, the effect of the perturbation introduced by the heave coupling is attenuated to an extent that allows the COM to be effectively used for model-based control design for the TMH.

Description of the Truth Model

The TM was developed by Bolender and Doman [3] and Groves et al. [17] as an attempt to extend earlier work done by Chavez and Schmidt [18]. It should be noted that [3] pertains to the richer truth model with heave coupling discussed later in this paper, whereas [17] addresses the TM specifically. In the present work, the total temperature change across the combustor input ΔT_0 used in [17] has been replaced with the functionally equivalent control input Φ, the fuel-to-air ratio. The change was made because Φ is a more natural input choice for aerospace systems and to avoid numerical scaling issues [3].

Figure 1 illustrates the basic geometry of the vehicle model, which incorporates only the longitudinal dynamics and assumes unit depth into the page. Because [3] offers an extensive explanation of the model derivation, only a brief summary of the employed techniques will be given here. Note that [3] also includes additional coupling effects that are not considered until later in this document. Rather than using the relatively simple approach of Newtonian Impact Theory [18], the model was derived using compressible flow theory. A combination of oblique shock and Prandtl–Meyer flow theory was used to determine the pressures across the range of possible angles of attack and structural bending conditions. The engine model is a scramjet taken directly from the paper by Chavez and Schmidt [18]. Because the angle of attack plays a significant role in determining the air flow properties into the scramjet engine, the thrust becomes heavily dependent on α. In addition, the underslung nature of the scramjet in this model produces a nose-up pitching moment directly proportional to thrust. The result is a loop interconnection between the propulsive and aerodynamic effects that must be carefully accounted for during control design. The model also includes flexible effects. For simplicity, the hypersonic vehicle (HSV) is modeled as a pair of cantilever beams, assumed to obey Hook's law, that are clamped at the craft's center of gravity. A derivation based on Lagrange's equations yields the equations of motion of the longitudinal dynamics for the HSV given by

$$\dot{h} = V\sin(\theta-\alpha) \qquad \dot{V} = \frac{1}{m}(T\cos\alpha - D) - g\sin(\theta-\alpha)$$

$$\dot{\alpha} = \frac{1}{mV}(-T\sin\alpha - L) + Q + \frac{g}{V}\cos(\theta-\alpha) \qquad \dot{\theta} = Q$$

$$I_{yy}\dot{Q} = M + \tilde{\psi}_1\ddot{\eta}_1 + \tilde{\psi}_2\ddot{\eta}_2$$

$$k_1\ddot{\eta}_1 = -2\zeta_1\omega_1\dot{\eta}_1 - \omega_1^2\eta_1 + N_1 - \tilde{\psi}_1\frac{M}{I_{yy}} - \frac{\tilde{\psi}_1\tilde{\psi}_2\ddot{\eta}_2}{I_{yy}}$$

$$k_2\ddot{\eta}_2 = -2\zeta_2\omega_2\dot{\eta}_2 - \omega_2^2\eta_2 + N_2 - \tilde{\psi}_2\frac{M}{I_{yy}} - \frac{\tilde{\psi}_2\tilde{\psi}_1\ddot{\eta}_1}{I_{yy}}$$

where the system state $x_{\mathrm{TM}} \in \mathbb{R}^9$ is composed of the nine state variables h, V, α, θ, Q, η_1, η_2, $\dot{\eta}_1$, and $\dot{\eta}_2$. Several physical constants derived from the vehicle geometry, aerodynamic conditions, and assumed elastic mode shapes are also included in the equations [3,17].

The control inputs** δ_e and Φ do not appear explicitly in the equations of motion. Instead, they enter through the forces and moments T, M, L, D, N_1, and N_2. Because the precise analytical expressions for the forces and moments are too complex to be included here, we refer the interested reader to [3] for details. The next section will begin by deriving a set of tractable approximations for these terms.

Derivation of the Curve-Fitted Model

The TM presented in the preceding section provides a rich model for simulation and verification of control design. If possible, the control law synthesis would begin by analyzing the structural properties of the truth model symbolically to determine its suitability for various nonlinear techniques. Unfortunately, direct application of nonlinear design methodologies such as feedback linearization to the TM governing equations is not possible. Indeed, several of the

**Because only two control inputs are required for functional controllability of the model, the additional input A_d used in [17] will be fixed at its nominal value $A_d = 1$ for the remainder of this study.

relevant equations are implicit functions of the state and input variables. Thus a closed-form representation of the system's vector field is not available. In addition, the lift, drag, thrust, pitching moment, and the two generalized forces are complex functions of both the system state and the inputs that must be simplified to render the model analytically tractable. Therefore, this section will proceed by deriving a simplified, closed-form model that retains the essential character of the TM.

Although attempts to represent the force mappings in the TM with cubic-spline interpolated lookup tables were very successful [21], these approximations are not suitable for symbolic analysis with the tools of geometric nonlinear control theory [22]. Thus, drawing on earlier work done with a nonflexible vehicle [11,13], the following approximations to these mappings will be adopted for this study:

$$
\begin{aligned}
L &\approx \frac{1}{2}\rho V^2 S C_L(\alpha, \delta_e) \qquad D \approx \frac{1}{2}\rho V^2 S C_D(\alpha, \delta_e) \\
M &\approx z_T T + \frac{1}{2}\rho V^2 S \bar{c}[C_{M,\alpha}(\alpha) + C_{M,\delta_e}(\delta_e)] \\
T &\approx C_T^{\alpha^3}\alpha^3 + C_T^{\alpha^2}\alpha^2 + C_T^{\alpha}\alpha + C_T^0 \\
N_1 &\approx N_1^{\alpha^2}\alpha^2 + N_1^{\alpha}\alpha + N_1^0 \\
N_2 &\approx N_2^{\alpha^2}\alpha^2 + N_2^{\alpha}\alpha + N_2^{\delta_e}\delta_e + N_2^0
\end{aligned}
\tag{1}
$$

The expressions for L and D are the same as those given in [13]. Note that the expression for M contains the additional term $z_T T$, where z_T is a known quantity, to account for the pitching moment produced by the underslung scramjet engine in the model [3]. The contribution of the pitch rate to the moment, which would be denoted $C_{M,Q}(\alpha, Q)$, has also been neglected, because it proved inconsequential for this vehicle. The numerical studies completed by Groves [21] support approximating the N_1 force as a quadratic function of the angle of attack and the N_2 force as a quadratic function of the angle of attack with a linear elevator deflection term. The forms for the functions appearing in Eqs. (1) and the generalized forces are selected as

$$
\begin{aligned}
C_L &= C_L^{\alpha}\alpha + C_L^{\delta_e}\delta_e + C_L^0 \\
C_D &= C_D^{\alpha^2}\alpha^2 + C_D^{\alpha}\alpha + C_D^{\delta_e^2}\delta_e^2 + C_D^{\delta_e}\delta_e + C_D^0 \\
C_{M,\alpha} &= C_{M,\alpha}^{\alpha^2}\alpha^2 + C_{M,\alpha}^{\alpha}\alpha + C_{M,\alpha}^0 \qquad C_{M,\delta_e} = c_e\delta_e \\
C_T^{\alpha^3} &= \beta_1(h,\bar{q})\Phi + \beta_2(h,\bar{q}) \qquad C_T^{\alpha^2} = \beta_3(h,\bar{q})\Phi + \beta_4(h,\bar{q}) \\
C_T^{\alpha} &= \beta_5(h,\bar{q})\Phi + \beta_6(h,\bar{q}) \qquad C_T^0 = \beta_7(h,\bar{q})\Phi + \beta_8(h,\bar{q})
\end{aligned}
\tag{2}
$$

where $\bar{q} = 1/2\rho V^2$ denotes dynamic pressure, and an exponential model of the form $\rho = \rho_0 \exp[-(h - h_0)/h_s]$ is adopted for the air density. The expressions for the lift, drag, and moment terms in Eqs. (2) are similar to those in [13], with minor notation changes and the addition of elevator terms in the lift and drag coefficients. The scramjet engine included in the model produces a thrust force T, which depends strongly on the states h, V, and α, along with the input Φ. The mapping is approximately cubic in the angle of attack, whereas each coefficient of this polynomial is a linear function of Φ. The eight $\beta_i(h, \bar{q})$ coefficients vary with the dynamic pressure and altitude. Because these values change on a much slower time scale than Φ and α, the values of β_i are assumed to be constant for control design. In implementation, the coefficients are obtained using a cubic-spline interpolated lookup table based on coefficients derived for 225 different flight conditions. Although functional forms for these β_i were derived, their use proved to be more cumbersome and less accurate than the use of lookup tables.

All the approximations given in Eqs. (2) are linear in their fit parameters. The values for S and $\bar{c}$ are known constants. The other parameters in Eqs. (2) have been obtained through a least-squares approach by fitting the functions to TM data calculated over the ranges given in Table 1. Naturally, the variation in $\bar{q}$ is obtained by appropriate variation of V. Even if a given force approximation does not explicitly depend on a particular state or input, that value will still be varied so as to capture its average effect. The flexible states η_i and $\dot{\eta}_i$ are set to zero during the calculation of the data for the least-squares fits, because their effects on the forces and moments are neglected in the selected approximations. The conditions within these ranges that are not physically realizable for the model are simply ignored by the curve-fitting algorithm. Figure 2 includes sample plots of aerodynamic data derived from the TM and the curve fits used by the control algorithms developed in the following sections ("Full Fit"). The generalized force fits are fairly accurate, but are omitted because they are not part of the COM developed in the sequel. The thrust and moment fits are almost exact matches with the truth model, due to the complexity of the functions used to approximate them, whereas the lift and drag fits capture only the general structure of the actual forces. Lift and drag fits with the elevator terms removed are also provided ("Simplified Fit" in the legend).

Table 1 Parameter ranges for curve fitting

Parameter	Lower bound	Upper bound
h	85,000 ft	135,000 ft
Φ	0.1	1.2
δ_e	−15 deg	15 deg
α	−10 deg	10 deg
$\bar{q}$	500 lb · ft^{-2}	2000 lb · ft^{-2}

Despite the simplifications that the CFM includes, the model mimics the dynamics of the TM with a reasonable degree of accuracy. Nevertheless, significant mismatch between the TM and the CFM does exist, particularly at extreme values of the system state. As a result, any control law designed on the basis of analytical models derived from the CFM will have to be robust to these modeling inaccuracies. Figure 3 shows the map of the poles and the transmission zeros of the Jacobian linearization of the TM and the CFM at the trim condition given in Table 2. The transmission zeros are computed with respect to the input $u = [\phi, \delta_e]$ and the output $y = [V, \gamma]$. For completeness, the CFM coefficient values corresponding to this trim condition are provided as an Appendix. The similarity between the two plots in Fig. 3 suggests that the curve fits capture the dominant terms in the TM's behavior around the considered trim condition. In particular, the CFM retains the nonminimum phase transmission zero that originates in the pitch dynamics, allowing an analysis based on the CFM to account for this effect in the TM. The resulting CFM remains complicated with significant couplings between the various subsystems. However, in this form, the behavior of the model can be studied analytically. In what follows, an analysis of the CFM will be provided using the tools of geometric control.

First, the structure of the CFM must be analyzed to determine what simplifications are required to arrive at the COM. One may calculate the relative degree of the CFM given in the preceding section, including both altitude and the four flexible states. Recall that the state $x_{\text{CFM}} \in \mathbb{R}^9$ contains the state variables discussed in the preceding section. The outputs were selected as $y_1 = V$ and $y_2 = \gamma$. Finally, the two control inputs are δ_e and Φ. For this input/output combination, the decoupling matrix $A(x_{\text{CFM}})$ of Lie derivatives is nonsingular over the range of interest, that is, the anticipated operating envelope given in Table 1. Unfortunately, the vector relative degree is only 2, meaning that the system possesses a 7-D internal dynamics with respect to the regulated output. The internal dynamics includes h, the pitch dynamics θ and Q, and the four flexible states.

The linearization around the trim condition given in Table 2 of both the TM and the CFM that are shown in Fig. 3 include seven zeros, as expected. The two complex conjugate pairs correspond to the flexible dynamics, indicating that they are minimum phase and supporting the decision to remove them from the COM as a first step in deriving the COM. The pair of zeros that appear to be symmetric about the $j\omega$ axis correspond to the pitch dynamics. These

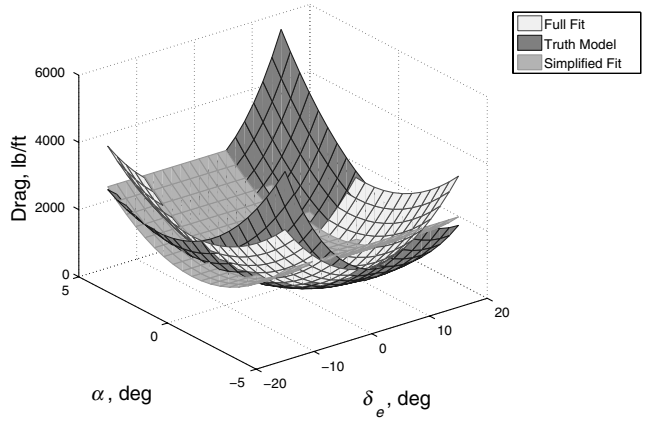

a) Drag fit sample plot

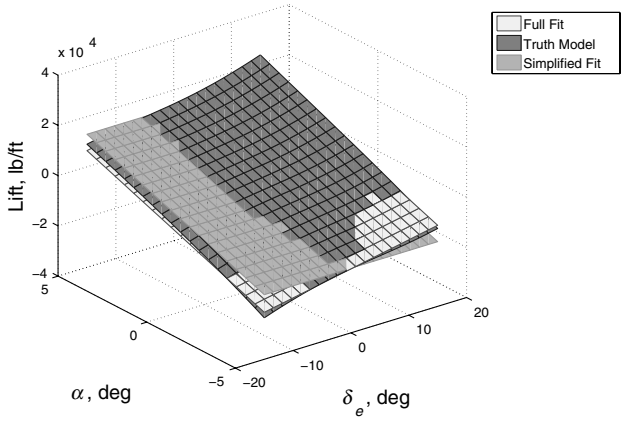

b) Lift fit sample plot

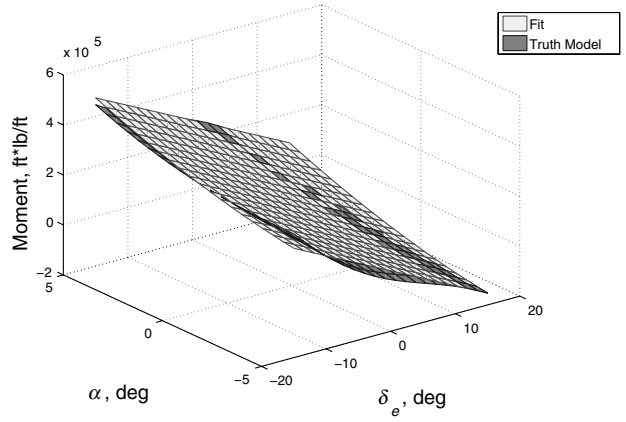

c) Moment fit sample plot

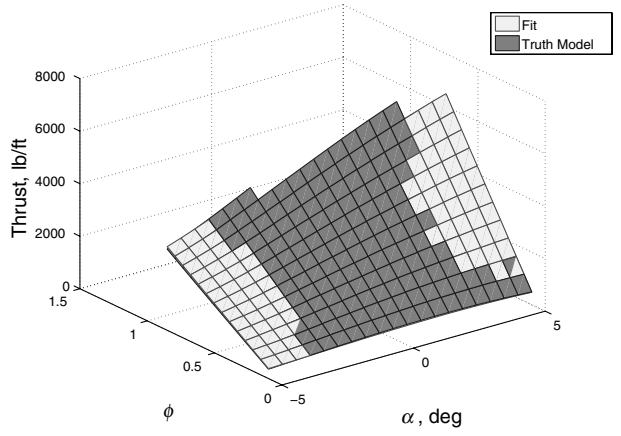

d) Thrust fit sample plot

Fig. 2 Sample plots of curve-fitting results.

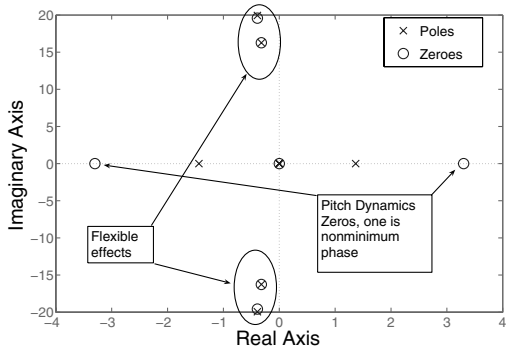

a) Truth model

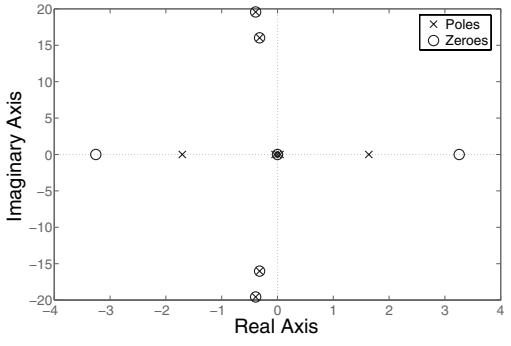

b) Curve-fitted model

Fig. 3 Pole/transmission zero maps of the Jacobian linearization of the TM and the CFM about the trim condition in Table 2. Input: $u = [\phi, \delta_e]$; output $y = [V, \gamma]$.

nonminimum phase dynamics will need to be addressed in the control design. The final zero resides at the origin and corresponds to the altitude state. This result should not be surprising, because the altitude dynamics behave as an undriven integrator when the output γ is forced to zero. The linearization also reveals that the plant is exponentially unstable, as evidenced by open-loop simulation results [3].

The nonminimum phase behavior of the model stems from the coupling of the elevator to the lift and drag forces. When the elevator is actuated to produce a nose-up moment, the aircraft experiences a loss of lift from the elevator [3]. Eventually, the angle of attack begins to change and overcomes this effect. This parasitic coupling is undesirable and responsible for the low relative degree of the model. By including this coupling, δ_e appears in lower-order derivatives of V and γ. By ignoring the weak elevator couplings, in particular setting to zero the terms $C_L^{\delta_e}$, $C_D^{\delta_e}$, and $C_D^{\delta_e^2}$ in Eq. (2), the nonminimum phase behavior can be removed from the model. Figure 2 shows the effect of neglecting these couplings on the curve fits for lift and drag. Although still present, these effects are dominated by the terms depending on α.

After removing the weak elevator couplings, the decoupling matrix $A(x)$ becomes singular over the operating range of interest. Thus, a dynamic extension [22] is required to obtain a model with vector relative degree. A second-order actuator model is appended to the input Φ, selecting the commanded value Φ_c as the new input,

$$\ddot{\Phi} = -2\zeta\omega\dot{\Phi} - \omega^2\Phi + \omega^2\Phi_c \tag{3}$$

Table 2 Trim condition for the truth model

State	Value	State	Value	Input	Value
h	85,000 ft	η_1	1.5122	ϕ	0.2514
V	7702.0808 ft $\cdot$ s^{-1}	$\dot{\eta}_1$	0	δ_e	11.4635 deg
α	1.5153 deg	η_2	1.2114		
θ	1.5153 deg	$\dot{\eta}_2$	0		
Q	0 deg $\cdot$s^{-1}				

Rather than simply adding a chain of two integrators, this choice has the added benefit of increasing the model fidelity by incorporating the lag associated with actuating Φ in a real vehicle. The actuator dynamics are chosen to impose a damping ratio $\zeta = 0.7$ and a natural frequency $\omega = 20$. With dynamic extension due to the appended actuator dynamics, symbolic calculations reveal that the COM has full vector relative degree 6 over the operating range of interest. Each output must be differentiated three times before an input appears, allowing the model to be decoupled into two chains of three integrators.

To summarize, the COM is obtained from the CFM by removing the altitude and flexible states and setting to zero the weak elevator couplings. A second-order dynamic extension is then added to Φ to obtain a 6-D model with full vector relative degree. The completed COM is given by the following set of equations:

$$\dot{V} = \frac{1}{m}(T\cos\alpha - D) - g\sin(\theta - \alpha)$$

$$\dot{\alpha} = \frac{1}{mV}(-T\sin\alpha - L) + Q + \frac{g}{V}\cos(\theta - \alpha) \qquad \dot{\theta} = Q$$

$$I_{yy}\dot{Q} = M$$

where

$$L = \frac{1}{2}\rho V^2 S C_L(\alpha, \delta_e) \qquad D = \frac{1}{2}\rho V^2 S C_D(\alpha, \delta_e)$$

$$M = z_T T + \frac{1}{2}\rho V^2 S\bar{c}[C_{M,\alpha}(\alpha) + C_{M,\delta_e}(\delta_e)]$$

$$T = C_T^{\alpha^3}\alpha^3 + C_T^{\alpha^2}\alpha^2 + C_T^{\alpha}\alpha + C_T^0$$

and

$$C_L = C_L^{\alpha}\alpha + C_L^0 \qquad C_D = C_D^{\alpha^2}\alpha^2 + C_D^{\alpha}\alpha + C_D^0$$

$$C_{M,\alpha} = C_{M,\alpha}^{\alpha^2}\alpha^2 + C_{M,\alpha}^{\alpha}\alpha + C_{M,\alpha}^0 \qquad C_{M,\delta_e} = c_e\delta_e$$

$$C_T^{\alpha^3} = \beta_1(h,\bar{q})\Phi + \beta_2(h,\bar{q}) \qquad C_T^{\alpha^2} = \beta_3(h,\bar{q})\Phi + \beta_4(h,\bar{q})$$

$$C_T^{\alpha} = \beta_5(h,\bar{q})\Phi + \beta_6(h,\bar{q}) \qquad C_T^0 = \beta_7(h,\bar{q})\Phi + \beta_8(h,\bar{q})$$

It should be emphasized that the eight β_i coefficients will be assumed to be constant when using the COM for design. In reality, these coefficients are functions of the relatively slow-changing variables h and $\bar{q}$, which are approximated by table lookup in simulation.

Analysis and Control-Oriented Modeling

Before any model-based controller can be designed (in particular, nonlinear inversion-based controllers), the relevant properties of the model in terms of its relative degree, functional controllability, and behavior of the internal dynamics must be analyzed. As mentioned briefly in the preceding section, a few additional simplifications will be made to arrive at a control-oriented version of the model.

Rather than selecting the output as $[V, h]$ as was done in numerous references [11,13,14], the output will be selected as $[V, \gamma]$. The choice of the flight path angle is more appropriate for use by an inner-loop controller or by a human pilot, whereas the altitude choice is more logical for use by a guidance loop. As mentioned earlier, the input is chosen as $u = [\delta_e, \Phi]$ to obtain a system having the same number of inputs and outputs. Intuitively, one would expect that the input δ_e will be primarily used to modulate the angle of attack (hence flight path angle), whereas Φ will be used to control the thrust, and hence velocity. This intuition will provide the key simplification used in the COM.

First, several states can be removed from the CFM without significantly reducing its fidelity. The altitude $h(t)$ changes at a very slow rate when compared to the other system states. Thus, for the purposes of control design, altitude will be assumed to be constant. The elimination of these dynamics will simplify the following calculations and has been shown in simulation to have very little impact on the controller performance. As a further simplification, the flexible states will be removed from the CFM. Because these modes are relatively weakly coupled to the rigid body modes, although only lightly damped, the design will not address them directly. The appropriateness of this assumption will be fully evaluated in simulation. When additional flexibility effects are added in the next section, additional measures will be required to reestablish consistence of the COM with the truth model. The following subsection will provide an analysis of the CFM using the tools of geometric control.

Control Design and Simulation Results for the Truth Model

The inner-loop control law will be designed using the COM. The results given in [23] and references therein suggest that this design will have the potential to perform well on the CFM and the TM, provided that the neglected coupling terms are sufficiently small. In the following subsections the control law will be derived and the simulation results for the TM will be observed.

Normal Form

The state of the COM comprises the four rigid body states V, α, θ, and Q along with the two states associated with the actuator dynamics (Φ and $\dot{\Phi}$). The input is selected as $[\delta_e, \Phi_c]$, whereas the output is given as $[V, \gamma]$. As explained in the preceding section, the COM has full vector relative degree, allowing a normal form to be explicitly derived [22,23]. The transformation in normal form was completed using a generic feedback linearization code for square multi-input/multi-output (MIMO) systems that was developed using Matlab symbolic toolbox. The system is rewritten in normal form by using the appropriate change of coordinates

$$z = \Gamma(x), \qquad \Gamma(x) = \begin{bmatrix} V & \mathcal{L}_f V & \mathcal{L}_f^2 V & \gamma & \mathcal{L}_f\gamma & \mathcal{L}_f^2\gamma \end{bmatrix}^T$$

to obtain the system

$$\dot{z}_1 = z_2 \qquad \dot{z}_2 = z_3 \qquad \dot{z}_3 = \mathcal{L}_f^3 V + \left(\mathcal{L}_{\Phi_c}\mathcal{L}_f^2 V\right)\Phi_c + \left(\mathcal{L}_{\delta_e}\mathcal{L}_f^2 V\right)\delta_e$$

$$\dot{z}_4 = z_5 \qquad \dot{z}_5 = z_6 \qquad \dot{z}_6 = \mathcal{L}_f^3\gamma + \left(\mathcal{L}_{\Phi_c}\mathcal{L}_f^2\gamma\right)\Phi_c + \left(\mathcal{L}_{\delta_e}\mathcal{L}_f^2\gamma\right)\delta_e$$

It should be noted that this structure is obtained as a direct result of the decision to eliminate the weak elevator couplings from the model. If the same coordinate change is performed with these couplings included, the system reads as

$$\dot{z}_1 = z_2 + (\mathcal{L}_{\delta_e}V)\delta_e \qquad \dot{z}_2 = z_3 + (\mathcal{L}_{\delta_e}\mathcal{L}_f V)\delta_e$$

$$\dot{z}_3 = \mathcal{L}_f^3 V + \left(\mathcal{L}_{\Phi_c}\mathcal{L}_f^2 V\right)\Phi_c + \left(\mathcal{L}_{\delta_e}\mathcal{L}_f^2 V\right)\delta_e$$

$$\dot{z}_4 = z_5 + (\mathcal{L}_{\delta_e}\gamma)\delta_e \qquad \dot{z}_5 = z_6 + (\mathcal{L}_{\delta_e}\mathcal{L}_f\gamma)\delta_e$$

$$\dot{z}_6 = \mathcal{L}_f^3\gamma + \left(\mathcal{L}_{\Phi_c}\mathcal{L}_f^2\gamma\right)\Phi_c + \left(\mathcal{L}_{\delta_e}\mathcal{L}_f^2\gamma\right)\delta_e$$

Designing a control law that accounts directly for the perturbation terms introduced into the first and second derivatives of the outputs by the elevator couplings is quite a challenging task, which goes beyond the scope of this work. Although this issue is currently being investigated, in this paper a simpler design approach based on approximate feedback linearization [15,23] will be pursued. According to the methodology in question, the weak coupling terms will simply be neglected, and a feedback linearization controller applied to the COM. Denoting by u_V and u_γ the outer-loop control

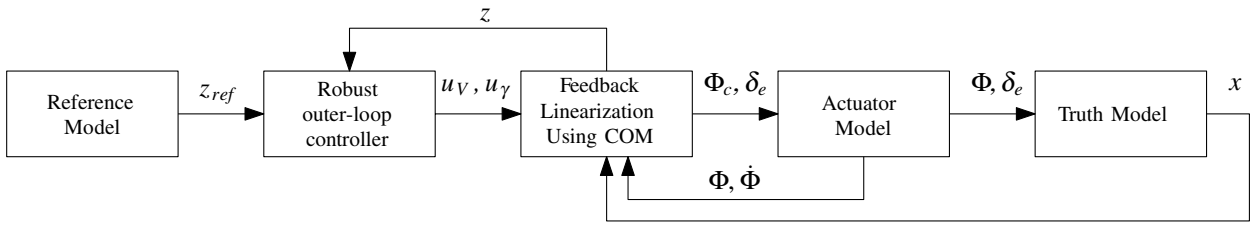

Fig. 4 Conceptual controller block diagram.

inputs, the control law

$$\begin{bmatrix} \Phi_c \\ \delta_e \end{bmatrix} = A(x)^{-1} \begin{bmatrix} u_V - \mathcal{L}_f^3 V \\ u_\gamma - \mathcal{L}_f^3 \gamma \end{bmatrix}, \qquad A(x) = \begin{bmatrix} \mathcal{L}_{\Phi_c}\mathcal{L}_f^2 V & \mathcal{L}_{\delta_e}\mathcal{L}_f^2 V \\ \mathcal{L}_{\Phi_c}\mathcal{L}_f^2 \gamma & \mathcal{L}_{\delta_e}\mathcal{L}_f^2 \gamma \end{bmatrix}$$

renders the input/output map of the COM linear, yielding

$$V^{(3)} = u_V \qquad \gamma^{(3)} = u_\gamma$$

The outer-loop linear controllers for the two decoupled integrator chains are designed using LQR with integral augmentation and a model reference. A conceptual block diagram of the controller is provided in Fig. 4. After a few trial-and-error iterations, the weights for the LQR cost function have been selected as

$$Q_V = \text{diag}(10, 1, 1, 1), \qquad R_V = 1, \qquad Q_\gamma = I_{4\times 4}$$
$$R_\gamma = 0.1$$

To obtain a reference model for each linear system, the reference signals for $V(t)$ and $\gamma(t)$ are filtered using fast low-pass filters with unity DC gain. The outputs of the reference model include $V_{\text{ref}}(t)$, $\gamma_{\text{ref}}(t)$, and higher-order derivatives. Denoting with K_V and K_γ the LQR design gains, the outer-loop controller is given by

$$u_V(t) = V_{\text{ref}}^{(3)} - K_V \begin{bmatrix} V - V_{\text{ref}} \\ \mathcal{L}_f V - \dot{V}_{\text{ref}} \\ \mathcal{L}_f^2 V - \ddot{V}_{\text{ref}} \\ \int_0^t [V(\tau) - V_{\text{ref}}(\tau)]\,\mathrm{d}\tau \end{bmatrix}$$

$$u_h(t) = h_{\text{ref}}^{(3)} - K_h \begin{bmatrix} h - h_{\text{ref}} \\ \mathcal{L}_f h - \dot{h}_{\text{ref}} \\ \mathcal{L}_f^2 h - \ddot{h}_{\text{ref}} \\ \int_0^t [h(\tau) - h_{\text{ref}}(\tau)]\,\mathrm{d}\tau \end{bmatrix}$$

The decoupling matrix $A(x)$ has been verified to be nonsingular over the operating range of interest, which is the range of parameter values used in the curve fits, and the controller is guaranteed by design to perform well on the COM. Simulations verify that the controller linearizes the COM up to the numerical accuracy of the algorithm used to integrate the nonlinear differential equations, provided that the variation of β_i is removed and the terms depending on h are held constant (recall that the slow variation of β_i with $\bar{q}$ and h is neglected in the control design.) Even with these variations in place, the input/output map from the outer-loop inputs to $[V, \gamma]$ is very nearly linear. Simulation results on the CFM demonstrate good tracking performance, as expected. These results will be omitted both for brevity and due to their similarity to the TM results, which are presented in the following subsection.

Truth Model Simulation Results

The truth model is implemented in Simulink using dedicated S-functions. All simulations used a variable step Dormand–Prince integration method with a maximum step size of 0.1 s. The selected reference trajectory begins at $\bar{q} = 2000$ lb $\cdot$ ft^{-2} and $h = 85,000$ ft. The aircraft climbs at a steady 50 ft $\cdot$ s^{-1}, while maintaining a constant dynamic pressure. Once the HSV reaches Mach 10 at time $t = 220$ s, the Mach number is held constant and the climb rate increases to 139 ft $\cdot$ s^{-1} until leveling off at 115,000 ft. This trajectory was determined to be a plausible operating trajectory for the vehicle, and the ramp increase in altitude provides a moderately aggressive tracking challenge to the controller. It should be noted that the available thrust limits the climb rate for this reference trajectory. If a faster climb rate is selected for the first leg, the required acceleration cannot be achieved without violating amplitude and rate limits on Φ (see [3]). The relationship $\dot{h}_{\text{ref}} = V_{\text{ref}} \sin(\gamma_{\text{ref}})$ is used to obtain the desired reference trajectory γ_{ref}, shown in Figs. 5a and 5b.

Figures 5c, 5d, and 6 show the simulation results for the test trajectory on the truth model under the proposed controller. The tracking performance is excellent throughout the entire maneuver, and both the flexible states and pitch dynamics remain stable and well-behaved. Although the tracking performance is also a result of the selection and filtering of the reference trajectory, the results demonstrate the effectiveness of the control law design. Figure 7 shows a simulation result for the truth model without the inclusion of integral augmentation. The tracking performance suffers significantly, particularly in the γ response, emphasizing the need for integrators in the outer loop to compensate for the mismatch between the COM and TM. Naturally, this controller uses different LQR tuning weights than those chosen for the controller with integral augmentation.

Heave Model Control Design

The original TM does not include heave coupling, which describes the excitation of the flexible effects by acceleration in the body axis normal direction, which is nearly equal to $\ddot{h}$ for small angles of attack. The more recent model includes these effects, along with a few other small modifications [3], and shall be denoted the truth model with heave coupling. The heave coupling significantly complicates the equations of motion. The body axis equations are given as

$$\dot{h} = U\sin\theta - W\cos\theta$$
$$m\dot{U} = -mQW - mg\sin\theta - \dot{Q}(\lambda_2\eta_2 - \lambda_1\eta_1) - 2Q(\lambda_2\dot{\eta}_2 - \lambda_1\dot{\eta}_1) + F_x$$
$$m\dot{W} = mQU + mg\cos\theta - \lambda_2\ddot{\eta}_2 - \lambda_1\ddot{\eta}_1 + Q^2(\lambda_2\eta_2 - \lambda_1\eta_1) + F_z$$
$$\left(I_{yy} + \eta_2^2 + \eta_1^2\right)\dot{Q} = -(\dot{U} + QW)(\lambda_2\eta_2 + \lambda_1\eta_1) - 2Q(\eta_2\dot{\eta}_2 + \eta_1\dot{\eta}_1) + \tilde{\psi}_2\ddot{\eta}_2 + \tilde{\psi}_1\ddot{\eta}_1 + M$$
$$\ddot{\eta}_1 = -(\dot{W} - QU)\lambda_1 + \dot{Q}\tilde{\psi}_1 - 2\zeta_1\omega_1\dot{\eta}_1 - \left(\omega_1^2 - Q^2\right)\eta_1 + N_1$$
$$\ddot{\eta}_2 = -(\dot{W} - QU)\lambda_2 + \dot{Q}\tilde{\psi}_2 - 2\zeta_2\omega_2\dot{\eta}_2 - \left(\omega_2^2 - Q^2\right)\eta_2 + N_2$$

These equations can be converted to the stability axis coordinate frame used in the preceding sections using the relations

$$\tan\alpha = W/U, \qquad V^2 = U^2 + W^2$$
$$L = F_x\sin\alpha - F_z\cos\alpha, \qquad D = -F_x\cos\alpha - F_z\sin\alpha$$

Unfortunately, the equations expressed in the stability frame are too lengthy to be included here and too cumbersome to be manipulated analytically. Because the flexible modes appear explicitly in the

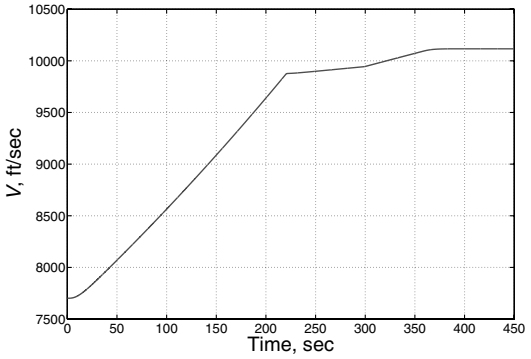

a) Reference trajectorty $V_{ref}(t)$

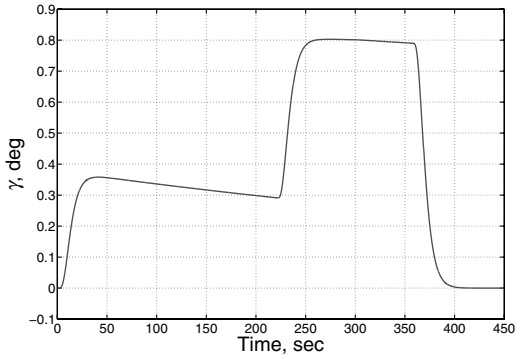

b) Reference trajectorty $\gamma_{ref}(t)$

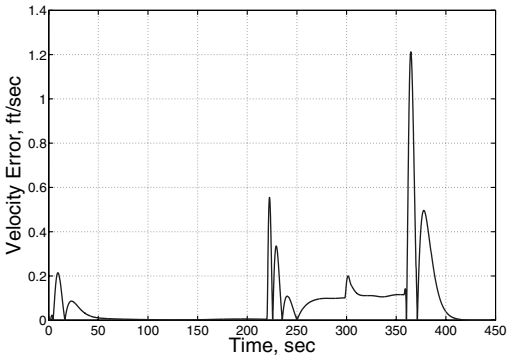

c) Tracking error $|V(t) - V_{ref}(t)|$

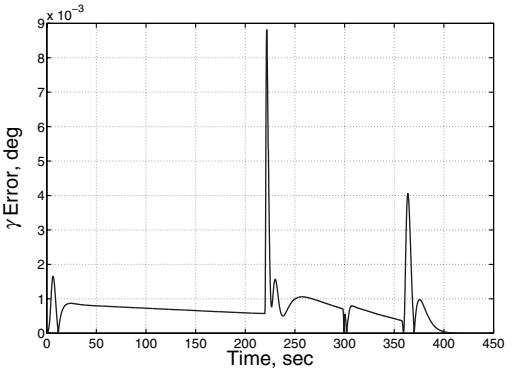

d) Tracking error $|\gamma(t) - \gamma_{ref}(t)|$

Fig. 5 Reference trajectories and simulation results for the truth model.

equations of motion, the complexity of the governing equations is substantially increased. The new level of interaction between the flexible modes and the rigid body dynamics severely affects the capability of the COM to approximate the TMH, up to the point that its use is no longer justified. As a matter of fact, the control law designed in the preceding section based on the COM results in instability when applied to the TMH, as seen in Fig. 8. It should be remarked that changing the weights of the outer-loop LQR controller

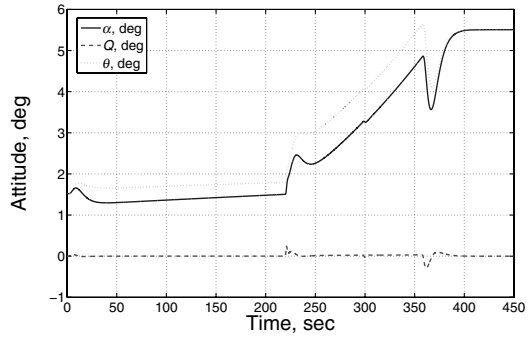

a) Angular states $\alpha(t)$, $\theta(t)$, $Q(t)$

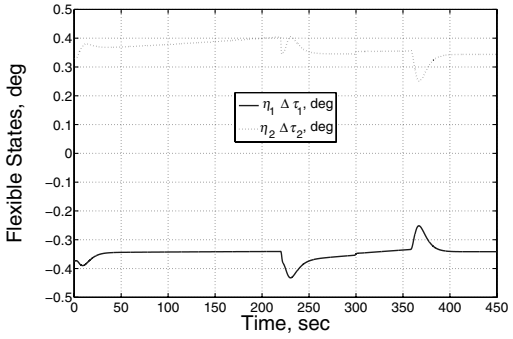

b) Flexible states $\eta(t)$, $\dot{\eta}(t)$

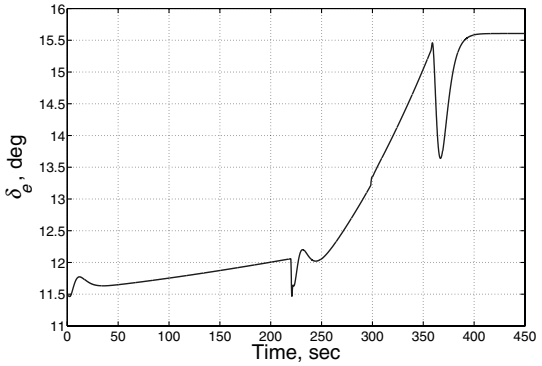

c) Control input $\delta_e(t)$

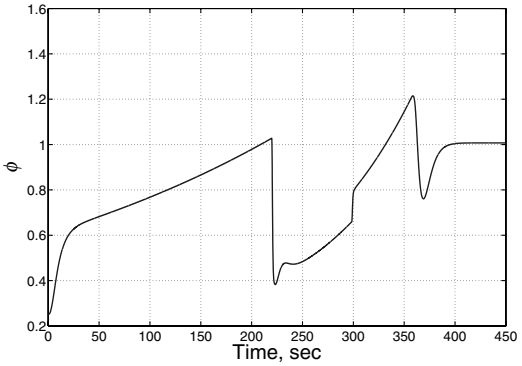

d) Control input $\Phi(t)$

Fig. 6 Simulation results for the truth model.

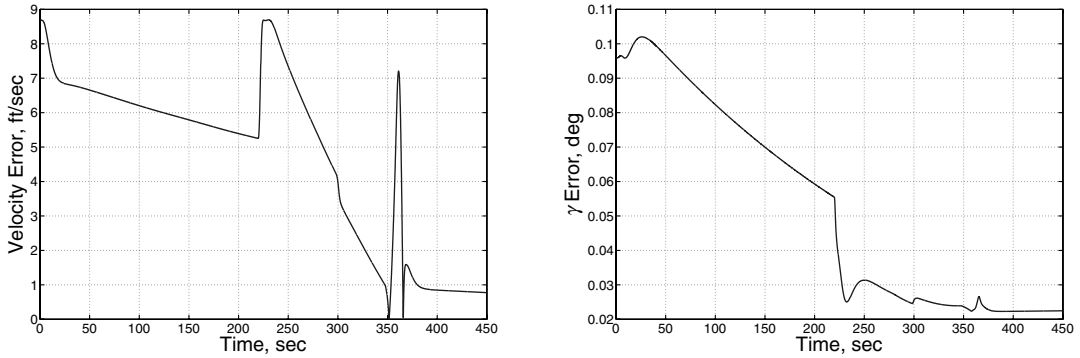

a) Tracking error $|V(t) - V_{\text{ref}}(t)|$ b) Tracking error $|\gamma(t) - \gamma_{\text{ref}}(t)|$

Fig. 7 Simulation result for the truth model without integral augmentation.

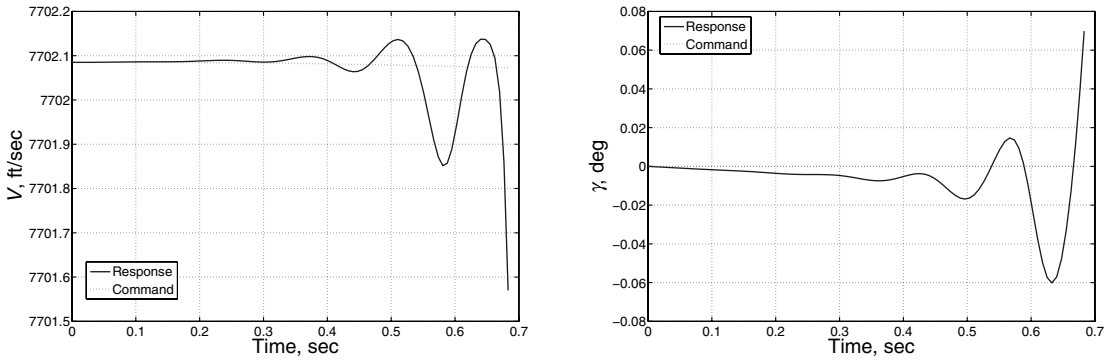

a) Velocity $V(t)$ and reference $V_{\text{ref}}(t)$ b) Flight-path angle $\gamma(t)$ and reference $\gamma_{\text{ref}}(t)$

Fig. 8 Simulation result for the truth model with heave coupling: original control law.

proved to be ineffective to achieving stabilization of the closed-loop system, a clear sign of severe model mismatch.

Preliminary Model Modification

The instability shown in Fig. 8 is the result of the more intricate coupling between the flexible and rigid dynamics, creating a highly unstable closed-loop aeroelastic mode inherited by the unstable zeros of the open-loop dynamics. The nonminimum phase behavior of the rigid modes results from the momentary loss of lift that occurs when the elevator is actuated to initiate a climb [20]. Because of the coupling with the flexible modes, this effect is significantly stronger than the one exhibited by the TM without heave coupling, and can no longer be neglected. It is postulated that reducing this nonminimum phase effect will contribute to alleviate the mismatch between the COM and the TMH. An additional effector can be used to compensate for the undesirable contribution of the elevator to lift, which appears in the equations as $C_L^{\delta_e}$, in such a way that it can be safely ignored in the COM. The strategy does not seek to directly impact the flexible modes. Instead, it is designed to render the rigid dynamics minimum phase, or as nearly so as possible, while at the same time providing additional control authority to the elevator to help suppress the unstable flexible oscillations that are observed in the TMH. For this study, a canard will be added to the airframe's forebody as discussed in [20]. The canard is placed near the nose of the aircraft, forward of the center of gravity as shown in Fig. 9. The deflection of the canard will be ganged with the elevator deflection using a negative gain. As a result, the lift contributions from these two effectors will have opposite signs, whereas their contributions to the moment will have the same sign. Thus, from the COM point of view, the coefficient $C_L^{\delta_e}$ will be made smaller, while $C_M^{\delta_e}$ will become larger. Because the COM assumed that $C_L^{\delta_e} = 0$, the interconnection gain k_{ec} between the canard and elevator will be chosen to cancel the lift contribution of the elevator as closely as possible. To proceed with the design, an additional curve fit of the lift force that included

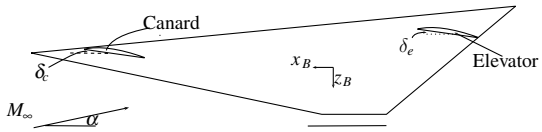

Fig. 9 Geometry of the hypersonic vehicle model with canard included.

the canard was completed. The functional form is given as

$$C_L = C_L^{\alpha}\alpha + C_L^{\delta_e}\delta_e + C_L^{\delta_c}\delta_c + C_L^0$$

where δ_c represents the canard deflection. Following the strategy outlined earlier, and in accordance with the derivation given in [20], the gain k_{ec} will be initially selected as

$$k_{\text{ec}} = -\frac{C_L^{\delta_e}}{C_L^{\delta_c}}$$

which, when $\delta_c = k_{\text{ec}}\delta_e$, results in

$$C_L = C_L^{\alpha}\alpha + C_L^0$$

Note that, according to this relation, and if the preceding intuition is correct, the addition of the canard should require little modifications to any controller designed on the basis of the COM, because it serves the purpose of canceling a term that the COM assumes to be zero. However, the canard also contributes to the moment and drag force. The drag contribution will be neglected in the COM, as is the drag contribution from the elevator. However, the moment contribution is significant and is included in the COM, because the canard is placed well forward of the vehicle's center of gravity. Therefore, a new curve fit of the moment force was performed as

$$C_{M,\delta_e} = c_e\delta_e + c_c\delta_c$$

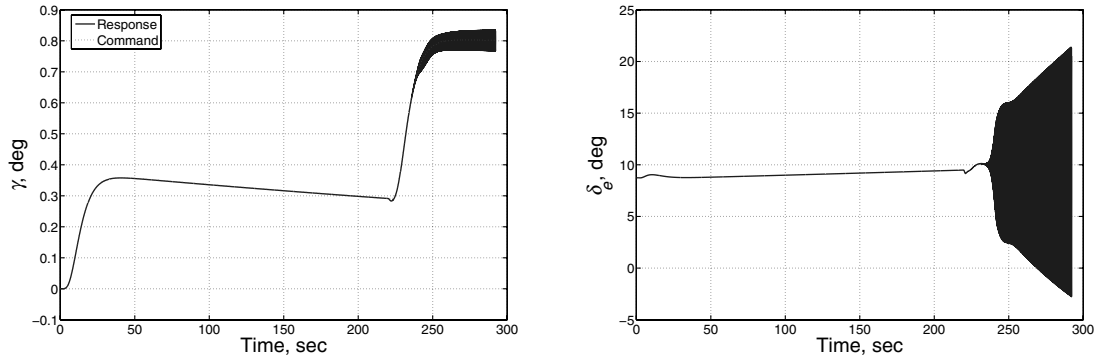

a) Flight-path angle $\gamma(t)$ and reference $\gamma_{\text{ref}}(t)$ b) Control input $\delta_e(t)$

Fig. 10 Simulation result for the TMH: canard gain $k_{\text{ec}} = -0.82$.

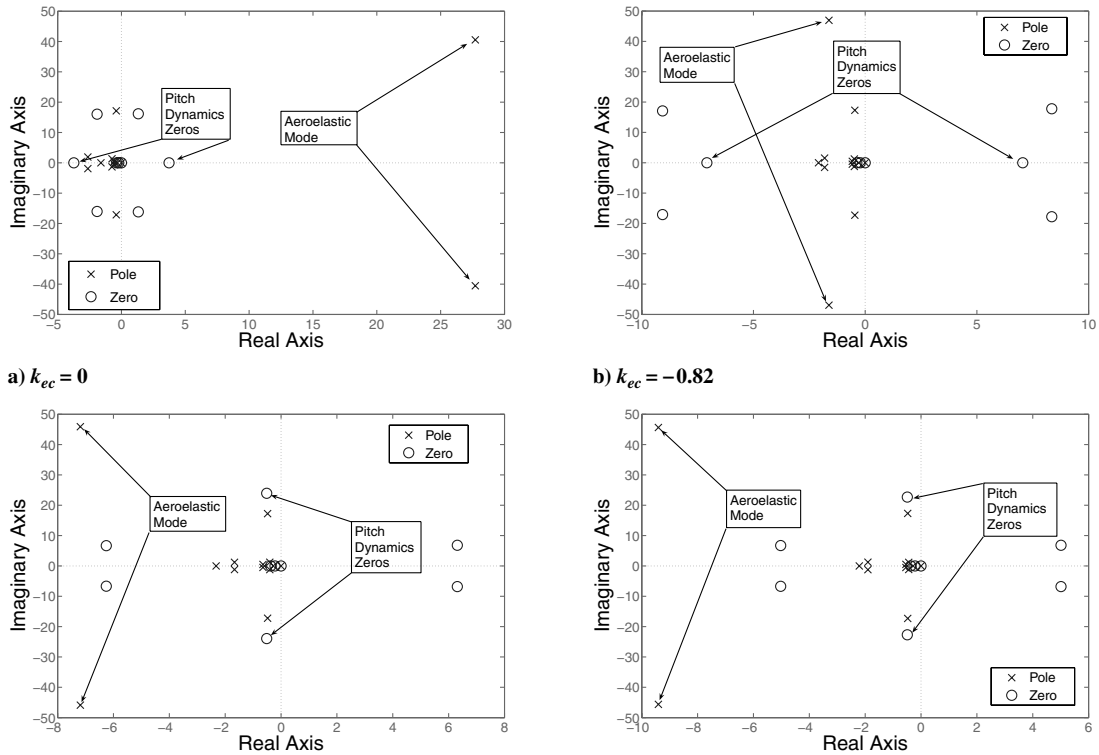

a) $k_{ec} = 0$ b) $k_{ec} = -0.82$

c) $k_{ec} = -1.2$ d) $k_{ec} = -1.5$

Fig. 11 Pole/transmission zero maps of the linearized closed-loop system for various values of k_{ec}. Input: $u = [\phi, \delta_e]$; output $y = [V, \gamma]$.

where the other moment terms remain the same. Thus, the original c_e term is simply changed to $c_e^{\text{new}} = c_e + k_{\text{ec}} c_c$.

COM Validation and TMH Controller

A viable approach to validate the approach and to fine tune k_{ec} is to evaluate the performance of the THM with canard in closed loop with the controller based on feedback linearization of the COM. Figure 10 gives the results obtained using the initial choice $k_{\text{ec}} = -0.82$. Unfortunately, whereas the controller performs well initially, it drives the plant into an unstable oscillation beginning around $t = 267$ s. To understand the reason for the instability observed with the $C_L^{\delta_e}$ term compensated, it is necessary to understand how the selection of k_{ec} also affects the flexible dynamics of the closed-loop system. It is speculated that the interaction of the flexible modes with the rigid body requires the gain k_{ec} to be chosen using other considerations than simple cancellation of $C_L^{\delta_e}$. The choice of k_{ec} to cancel the lift contribution of the elevator was made purely from an analysis of the zero dynamics of the rigid body. As already discussed, the interaction of the flexible modes with the rigid body creates an aeroelastic mode that is unstable without a canard. The behavior of this mode as a function of k_{ec} must be explored to determine why the gain $k_{\text{ec}} = -0.82$ was not successful.

Figure 11 shows the pole zero map of the closed-loop system for four different values of k_{ec}. The linearization is performed with the dynamic inversion inner loop and the LQR outer loop in place, but with the reference model removed and the reference inputs chosen as the desired setpoint. First, notice that there are nine zeros: four coming from the flexible states, two originating with the pitch dynamics, and the zero at the origin corresponding to altitude. The two additional minimum phase zeros are from the error integrators included in the outer-loop LQR controller. The features of interest on these plots are the pair of poles marked as the aeroelastic mode and the pitch dynamics zeros. When $k_{\text{ec}} = 0$, one of the pitch zeros is nonminimum phase, and the aeroelastic mode is extremely unstable. The addition of a canard with $k_{\text{ec}} = -0.82$ partially alleviates these problems. The aeroelastic mode becomes stable, although it remains fairly close to the $j\omega$ axis. At the same time, as expected [20], the pitch zeros are forced farther away from the $j\omega$ axis and likely out of the control bandwidth. Nevertheless, they remain real-valued and

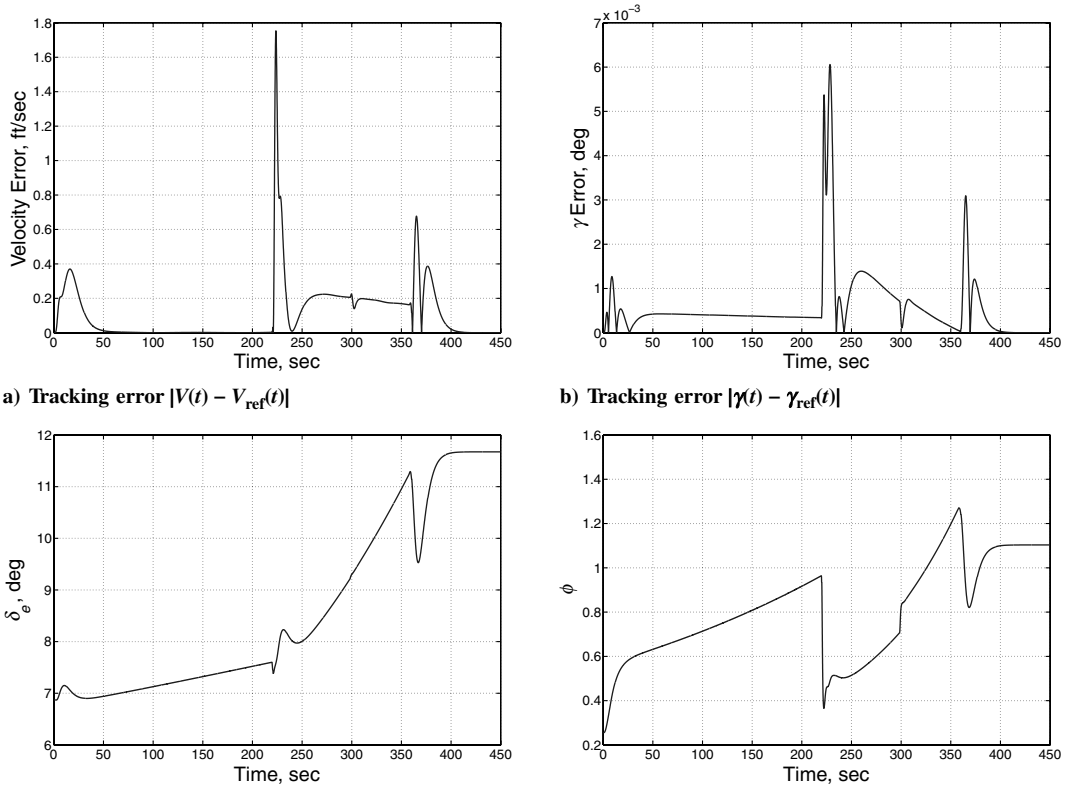

a) Tracking error $|V(t) - V_{ref}(t)|$ b) Tracking error $|\gamma(t) - \gamma_{ref}(t)|$

c) Control input $\delta_e(t)$ d) Control input $\Phi(t)$

Fig. 12 Simulation result for the TMH: canard gain $k_{ec} = -1.5$.

nonminimum phase. It is also interesting to note that the addition of the canard changes the imaginary component of the aeroelastic mode, due to the stronger interaction between the elevator and the pitch dynamics induced by the canard ganging. Increasing the magnitude of the canard actuation to $k_{ec} = -1.2$ causes the pitch dynamics zeros to migrate into a stable complex conjugate pair and increases the stability margin of the aeroelastic mode. Selecting $k_{ec} = -1.5$ increases the stability of the aeroelastic mode even further, but also brings the three pairs of complex conjugate zeros closer to the imaginary axis.

To summarize these observations, increasing the magnitude of k_{ec} lessens and eventually eliminates the nonminimum phase character of the pitch dynamics while also serving to stabilize the aeroelastic mode with an ever-increasing stability margin. However, increasing this value also moves the zeros associated with the flexible effects closer to the $j\omega$ axis. A compromise was reached between these effects by selecting $k_{ec} = -1.5$. It should be noted that this analysis is based solely on linearization about a single trim condition for the plant. Thus, even though this linearization was stable for $k_{ec} = -0.82$, nearness of the aeroelastic poles to the $j\omega$ axis makes it unsurprising that the full nonlinear TMH can become unstable under dynamic inversion. The choice of larger k_{ec} prevents the unstable oscillations from developing by increasing the stability margins. It should be emphasized that the elevator itself is unchanged. The additional control authority stems from the additional force produced by the coordinated actuation of the canard.

Figure 12 shows the simulation results for $k_{ec} = -1.5$ on the TMH. This choice of the canard ganging gain allows successful tracking of the reference trajectory that is comparable to the results achieved on the TM without heave coupling.

Parameter Variation Case Study

The control law designed for the TMH includes a robust outer-loop LQR along with integral augmentation. As a result, the design is moderately insensitive to plant parameter variations. Although an exhaustive attempt to verify and validate this design was not pursued, a few test cases were provided to qualitatively assess the robustness of the approach. For simplicity, only the moment of inertia I_{yy}, the vehicle length L_v, and the mass m will be varied. As a result of fuel consumption and thermal expansion of the aircraft during flight, these quantities will probably vary during the course of a typical mission. Thus, any practical controller designed for a HSV would need to be resistant to small deviations of these parameters from their nominal values. The test trajectory will be the one used in all previous simulations to simplify comparison of the results. Table 3 gives the parameter values for the three test cases, along with the nominal parameter values and the values of the key stability derivatives at trim.

In Fig. 13, simulation results for case 1 and case 2 are compared with those obtained for the nominal model. Notice that the reduction in vehicle mass and pitching moment for case 1 results in lower required control energy, as expected. Although the tracking error performance is inferior to the nominal parameter case, the control law still tracks the entire reference with nearly negligible tracking error. The results for case 2 reveal that the increases in mass and moment

Table 3 Test cases for parameter variation simulations

Case	L_v	$I_{yy} \times 10^5$	m	$\partial L/\partial\alpha \times 10^6$	$\partial M/\partial\alpha \times 10^8$
Nominal	100 ft	5 lb · ft	300 lb · ft^{-1}	8.3631 lb · ft^{-1} · deg^{-1}	1.2470 lb · ft · deg^{-1}
1	90 ft	4 lb · ft	240 lb · ft^{-1}	7.4089 lb · ft^{-1} · deg^{-1}	0.0741 lb · ft · deg^{-1}
2	110 ft	6 lb · ft	300 lb · ft^{-1}	9.1746 lb · ft^{-1} · deg^{-1}	1.7063 lb · ft · deg^{-1}
3	50 ft	4 lb · ft	150 lb · ft^{-1}	4.3707 lb · ft^{-1} · deg^{-1}	−0.0657 lb · ft · deg^{-1}

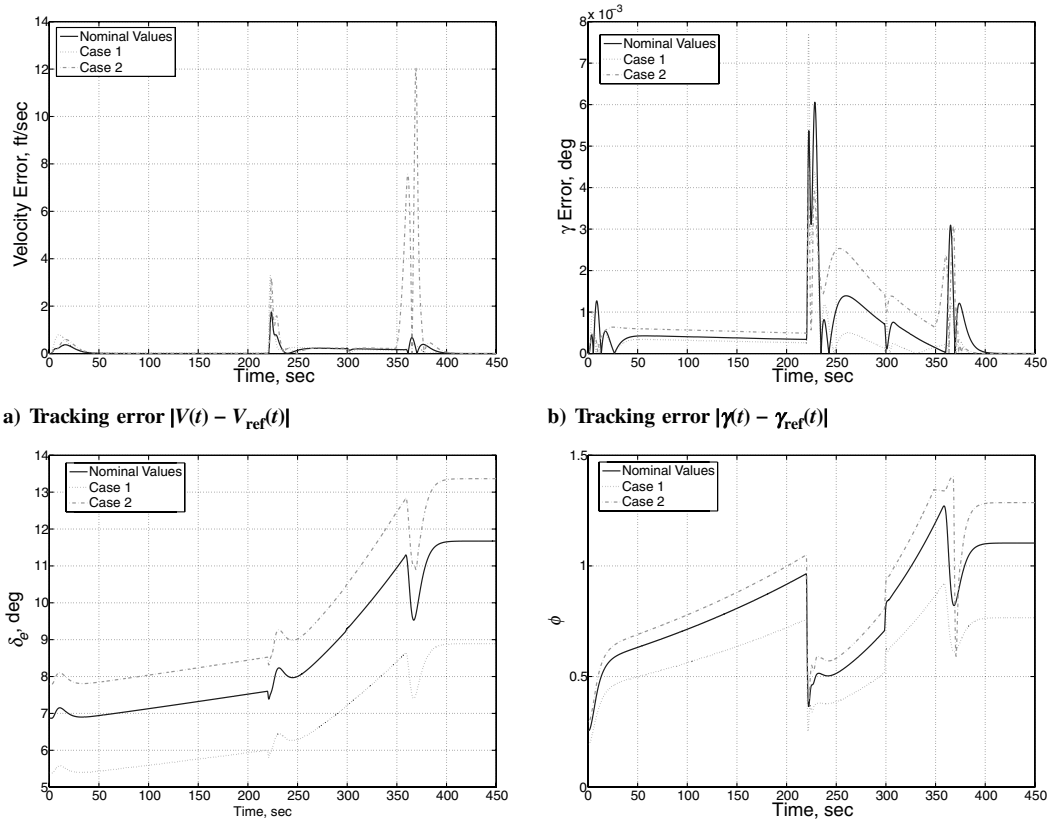

a) Tracking error $|V(t) - V_{ref}(t)|$

b) Tracking error $|\gamma(t) - \gamma_{ref}(t)|$

c) Control input $\delta_e(t)$

d) Control input $\Phi(t)$

Fig. 13 Comparison of simulation results for parameter variation case study in Table 1.

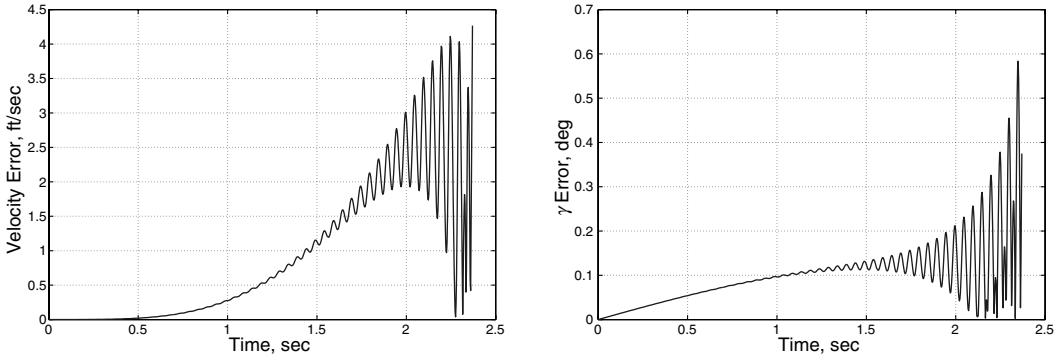

a) Tracking error $|V(t) - V_{ref}(t)|$

b) Tracking error $|\gamma(t) - \gamma_{ref}(t)|$

Fig. 14 Simulation result for parameter variation case 3.

require additional control energy from both the elevator and engine. Because the vehicle is thrust-limited, further increases in these values, particularly mass, render the reference trajectory infeasible for the aircraft. Finally, the extreme parameter variation of case 3 results in instability as observed in Fig. 14. The main challenge presented to the control system by these three test cases is the variation in vehicle length. As the aircraft becomes shorter, damping of the flexible modes is reduced. Eventually, the aeroelastic coupling with the rigid modes causes the system to become unstable. Overall, this brief study indicates that the control law is robust to mild plant parameter variations.

It should be emphasized that this brief case study is not an attempt to validate this design for practical use. The focus of this study is the control-oriented modeling of a hypersonic vehicle. Once the properties of the model, and the required model fidelity to obtain adequate controller performance, are clearly understood, then detailed nonlinear control designs can be developed. At that point, an extensive design process that incorporates robustness in its formulation can be pursued. The results in this section merely serve to illustrate that a qualitative degree of robustness is achieved by the included design without including this objective directly in the problem formulation.

Conclusions

This paper has explored control-oriented modeling of an air-breathing hypersonic vehicle. Whereas earlier works dealt with models that could be directly feedback-linearized, the truth models in this document were not symbolically tractable. By developing approximations to complex expressions and neglecting slow dynamics and weak couplings, intractably complex models can be rendered amenable to using nonlinear control methods. Although this modeling phase is time-consuming and results in a significantly more complex control law, this approach does not require gain scheduling or other similar techniques that would accompany a linear control approach. Also, the design of the outer-loop controller is

greatly simplified by inner-loop dynamic inversion techniques, and the design of the inner loop itself is completely standard once a suitable model is obtained. Thus, the nonlinear approach results in a simpler design process, albeit at the expense of additional modeling effort. An added benefit resulting from the effort spent in developing the control-oriented model is a thorough understanding of the system-theoretic properties of the system. The analysis of the zero dynamics of a more complex truth models with added coupling between the flexible modes and the rigid body modes led to the decision to include an additional control surface, namely, a canard. The canard helps to eliminate the nonminimum phase behavior of the rigid dynamics and results in stabilization of a high-frequency aeroelastic mode introduced by the heave coupling. The control design process provided insights on the vehicle design, just as modifications to the model required adjustments to the control algorithm. These interactions highlight the benefits of control-oriented modeling carried out in conjunction with the early phases of vehicle design.

Table A1 Miscellaneous coefficient values

Coefficient	Value	Units
S	1.7000×10^{1}	$\text{ft}^2 \cdot \text{ft}^{-1}$
ρ_0	6.7429×10^{-5}	$\text{slugs} \cdot \text{ft}^{-3}$
h_0	8.5000×10^{4}	ft
h_s	2.1358×10^{4}	ft

Table A2 Lift and drag coefficient values

Coefficient	Value	Units
C_L^{α}	4.6773×10^{0}	rad^{-1}
$C_L^{\delta_e}$	7.6224×10^{-1}	rad^{-1}
C_L^{0}	-1.8714×10^{-2}	——

Table A3 Drag coefficient values

Coefficient	Value	Units
$C_D^{\alpha^2}$	5.8224×10^{0}	rad^{-2}
C_D^{α}	-4.5315×10^{-2}	rad^{-1}
$C_D^{\delta_e^2}$	8.1993×10^{-1}	rad^{-2}
$C_D^{\delta_e}$	2.7699×10^{-4}	rad^{-1}
C_D^{0}	1.0131×10^{-2}	——

Table A4 Moment coefficient values

Coefficient	Value	Units
z_T	8.3600×10^{0}	ft
$\bar{c}$	1.7000×10^{1}	ft
$C_{M,\alpha}^{\alpha^2}$	6.2926×10^{0}	rad^{-2}
$C_{M,\alpha}^{\alpha}$	2.1335×10^{0}	rad^{-1}
$C_{M,\alpha}^{0}$	1.8979×10^{-1}	——
c_e	-1.2897×10^{0}	rad^{-1}

Table A5 Thrust coefficient values

Coefficient	Value	Units
β_1	-3.7693×10^{5}	$\text{lb} \cdot \text{ft}^{-1} \cdot \text{rad}^{-3}$
β_2	-3.7225×10^{4}	$\text{lb} \cdot \text{ft}^{-1} \cdot \text{rad}^{-3}$
β_3	2.6814×10^{4}	$\text{lb} \cdot \text{ft}^{-1} \cdot \text{rad}^{-2}$
β_4	-1.7277×10^{4}	$\text{lb} \cdot \text{ft}^{-1} \cdot \text{rad}^{-2}$
β_5	3.5542×10^{4}	$\text{lb} \cdot \text{ft}^{-1} \cdot \text{rad}^{-1}$
β_6	-2.4216×10^{3}	$\text{lb} \cdot \text{ft}^{-1} \cdot \text{rad}^{-1}$
β_7	6.3785×10^{3}	$\text{lb} \cdot \text{ft}^{-1}$
β_8	-1.0090×10^{2}	$\text{lb} \cdot \text{ft}^{-1}$

Table A6 N_1 coefficient values

Coefficient	Value	Units
$N_1^{\alpha^2}$	1.4013×10^{3}	$\text{lb} \cdot \text{ft}^{-1} \cdot \text{slug}^{-0.5} \cdot \text{rad}^{-2}$
N_1^{α}	4.5737×10^{3}	$\text{lb} \cdot \text{ft}^{-1} \cdot \text{slug}^{-0.5} \cdot \text{rad}^{-1}$
N_1^{0}	1.1752×10^{2}	$\text{lb} \cdot \text{ft}^{-1} \cdot \text{slug}^{-0.5}$

Table A7 N_2 coefficient values

Coefficient	Value	Units
$N_2^{\alpha^2}$	-5.0227×10^{3}	$\text{lb} \cdot \text{ft}^{-1} \cdot \text{slug}^{-0.5} \cdot \text{rad}^{-2}$
N_2^{α}	2.8633×10^{3}	$\text{lb} \cdot \text{ft}^{-1} \cdot \text{slug}^{-0.5} \cdot \text{rad}^{-1}$
$N_2^{\delta_e}$	1.2465×10^{3}	$\text{lb} \cdot \text{ft}^{-1} \cdot \text{slug}^{-0.5} \cdot \text{rad}^{-1}$
N_2^{0}	-4.4201×10^{1}	$\text{lb} \cdot \text{ft}^{-1} \cdot \text{slug}^{-0.5}$

Appendix

Tables A1–A7 provide the coefficients for the CFM corresponding to the trim condition given in Table 2. With the exception of the eight β_i thrust coefficients, which vary with h and $\bar{q}$, these values are used for all flight conditions.

Acknowledgements

This work has been supported by U.S. Air Force Research Laboratories—Air Vehicles Directorate and U.S. Air Force Office of Scientific Research through the Collaborative Center of Control Science at The Ohio State University (Contract F33615-01-2-3154.) This material is based upon work supported under a National Science Foundation Graduate Research Fellowship. Any opinions, findings, conclusions or recommendations expressed in this publication are those of the author(s) and do not necessarily reflect the views of the National Science Foundation. We would also like to thank Pete Jankovsky at The Ohio State University for completing many of the curve fits used in the synthesis of the controller.

References

[1] Schmidt, D. K., "Dynamics and Control of Hypersonic Aeropropulsive/Aeroelastic Vehicles," AIAA Paper 1992-4326, 1992.

[2] Schmidt, D. K., "Integrated Control of Hypersonic Vehicles—A Necessity Not Just a Possibility," AIAA Paper 1993-3761, 1993, pp. 539–549.

[3] Bolender, M. A., and Doman, D. B., "A Non-Linear Model for the Longitudinal Dynamics of a Hypersonic Air-Breathing Vehicle," AIAA Paper 2005-6255, 2005.

[4] McRuer, D., "Design and Modeling Issues for Integrated Airframe/Propulsion Control of Hypersonic Flight Vehicles," *Proceedings of the American Control Conference*, American Automatic Control Council, Evanston, IL, 1992, pp. 729–734.

[5] Bilimoria, K., and Schmidt, D., "Integrated Development of the Equations of Motion for Elastic Hypersonic Flight Vehicles," *Journal of Guidance, Control, and Dynamics*, Vol. 18, No. 1, 1995, pp. 73–81.

[6] Schmidt, D. K., and Velapoldi, J. R., "Flight Dynamics and Feedback Guidance Issues for Hypersonic Airbreathing Vehicles," AIAA Paper 1999-4122, 1999.

[7] Schmidt, D., "Optimum Mission Performance and Multivariable Flight Guidance for Airbreathing Launch Vehicles," *Journal of Guidance, Control, and Dynamics*, Vol. 20, No. 6, 1997, pp. 1157–1164.

[8] Davidson, J., Lallman, F., McMinn, J. D., Martin, J., Pahle, J., Stephenson, M., Selmon, J., and Bose, D., "Flight Control Laws for NASA's Hyper-X Research Vehicle," AIAA Paper 1999-4124, 1999.

[9] Tournes, C., Landrum, D. B., Shtessel, Y., and Hawk, C. W., "Ramjet-Powered Reusable Launch Vehicle Control by Sliding Modes," *Journal of Guidance, Control, and Dynamics*, Vol. 21, No. 3, 1998, pp. 409–415.

[10] Doman, D. B., and Ngo, A. D., "Dynamic Inversion-Based Adaptive/Reconfigurable Control of the X-33 on Ascent," *Journal of Guidance, Control, and Dynamics*, Vol. 25, No. 2, 2002, pp. 275–284.

[11] Wang, Q., and Stengel, R., "Robust Nonlinear Control of a Hypersonic Aircraft," *Journal of Guidance, Control, and Dynamics*, Vol. 23, No. 4, 2000, pp. 577–585.

[12] Marrison, C., and Stengel, R., "Design of Robust Control Systems for a Hypersonic Aircraft," *Journal of Guidance, Control, and Dynamics*, Vol. 21, No. 1, 1998, pp. 58–63.
[13] Xu, H., Mirmirani, M., and Ioannou, P., "Adaptive Sliding Mode Control Design for a Hypersonic Flight Vehicle," *Journal of Guidance, Control, and Dynamics*, Vol. 27, No. 5, 2004, pp. 829–838.
[14] Parker, J. T., Serrani, A., Yurkovich, S., Bolender, M. A., and Doman, D. B., "Approximate Feedback Linearization of an Air-Breathing Hypersonic Vehicle," AIAA Paper 2006-6556, 2006.
[15] Hauser, J., Sastry, S., and Meyer, G., "Nonlinear Control Design for Slightly Nonminimum Phase Systems: Application to V/STOL Aircraft," *Automatica*, Vol. 28, No. 4, 1992, pp. 665–679.
[16] Isidori, A., Marconi, L., and Serrani, A., "Robust Nonlinear Motion Control of a Helicopter," *IEEE Transactions on Automatic Control*, Vol. 48, No. 3, 2003, pp. 413–426.
[17] Groves, K. P., Sigthorsson, D. O., Serrani, A., Yurkovich, S., Bolender, M. A., and Doman, D. B., "Reference Command Tracking for a Linearized Model of an Air-Breathing Hypersonic Vechicle," AIAA Paper 2005-6144, 2005.
[18] Chavez, F., and Schmidt, D., "Analytical Aeropropulsive/Aeroelastic Hypersonic-Vehicle Model with Dynamic Analysis," *Journal of Guidance, Control, and Dynamics*, Vol. 17, No. 6, 1994, pp. 1308–1319.
[19] Chavez, F., and Schmidt, D., "Uncertainty Modeling for Multivariable Control Robustness Analysis of Elastic High-Speed Vehicles," *Journal of Guidance, Control, and Dynamics*, Vol. 22, No. 1, 1999, pp. 87–95.
[20] Bolender, M., and Doman, D., "Flight Path Angle Dynamics of Air-Breathing Hypersonic Vehicles," AIAA Paper 2006-6692, 2006.
[21] Groves, K. P., "Modelling, Simulation, and Control Design of an Air-Breathing Hypersonic Vehicle," M.S. Thesis, The Ohio State University, Columbus, OH, July 2005.
[22] Isidori, A., *Nonlinear Control Systems*, Springer–Verlag, Berlin, 1989.
[23] Sastry, S., *Nonlinear Systems Analysis, Stability, and Control*, Springer, New York, 1999.